

Influence of Bond Coat on HVOF-Sprayed Gradient Cermet Coating on Copper Alloy

Peng Ke^{1,2} · Fei Cai² · Wanglin Chen^{1,2} · Shuoyu Wang³ · Zhenhang Ni³ · Xiaohong Hu³ · Mingxi Li¹ · Guanghong Zhu³ · Shihong Zhang^{1,2}

Submitted: 4 November 2016/in revised form: 20 February 2017/Published online: 25 May 2017
© ASM International 2017

Abstract Coatings are required on mold copper plates to prolong their service life through enhanced hardness, wear resistance, and oxidation resistance. In the present study, NiCr-30 wt.%Cr₃C₂ ceramic–metallic (cermet) layers were deposited by high velocity oxy-fuel (HVOF) spraying on different designed bond layers, including electroplated Ni, HVOF-sprayed NiCr, and double-decker Ni-NiCr. Annealing was also conducted on the gradient coating (GC) with NiCr bond layer to improve the wear resistance and adhesion strength. Coating microstructure was investigated by scanning electron microscopy and x-ray diffraction analysis. Mechanical properties including microhardness, wear resistance, and adhesion strength of the different coatings were evaluated systematically. The results show that the types of metallic bond layer and annealing process had a significant impact on the mechanical properties of the GCs. The GCs with electroplated Ni bond layer exhibited the highest adhesion strength (about 70 MPa). However, the GC with HVOF-sprayed NiCr bond layer exhibited better wear resistance. The wear resistance and adhesion strength of the coating

with NiCr metallic bond layer were enhanced after annealing.

Keywords adhesion strength · gradient coatings · HVOF · wear resistance

Introduction

The mold copper plate (MCP) is an important part of continuous casting equipment, enabling rapid solidification by transferring heat from liquid steel to cooling water (Ref 1). The inner surface of the MCP is subject to intensive wear and severe high-temperature conditions simultaneously, resulting in demanding requirements in terms of wear resistance and thermal stability such as high-temperature strength and oxidation resistance (Ref 2). In past decades, electroplating of a chromium layer of certain thickness has been widely applied on MCPs to improve their mechanical performance. Such an electroplated chromium layer indeed improves the service life of MCPs and thereby increases production efficiency. However, due to their inherent brittleness and formation of microcracks, such layers have gradually been replaced by electroplated NiCoW or NiCo layers (Ref 3, 4).

High velocity oxy-fuel (HVOF) spraying has drawn great attention in industry due to its superior ability for deposition of hard coatings (Ref 5, 6). Because of their much higher hardness and further enhanced wear resistance and oxidation resistance compared with electroplating coatings (Ref 7-9), such hard coatings have been widely applied to improve the lifetime of different metallurgical parts such as stable rollers, sink rollers, and continuous casting rolls (Ref 10-12). The adhesion strength of HVOF coatings sprayed onto CrZrCu substrate is relative low,

✉ Shihong Zhang
tougayouxiang206@163.com

¹ School of Materials Science and Engineering, Anhui University of Technology, Maanshan City 243002, Anhui Province, People's Republic of China

² Research Center of Modern Surface and Interface Engineering, Anhui University of Technology, Maanshan City 243002, Anhui Province, People's Republic of China

³ Maanshan Ma Steel Surface Engineering Technology Co. Ltd., Maanshan 243000, People's Republic of China

greatly limiting application of the HVOF method on MCPs (Ref 13), but few investigations have focused on this issue. This lower adhesion strength is mainly due to the physical characteristics of ceramic coatings, such WC-Co or NiCr-Cr₃C₂ ceramic-metallic coatings, which differ obviously from those of the Cu matrix, which can result in notable interfacial stress concentrations due to the difference between their thermal expansion coefficient, crystal structure, and hardness. Use of gradient coating (GC) structure is proposed herein to resolve these problems.

WC-Co and NiCr-Cr₃C₂ HVOF ceramic-metallic coatings are extensively used for wear- and corrosion-resistant applications (Ref 14–16). WC-Co ceramic-metallic coatings generally exhibit high hardness and wear resistance, but WC will decarburize to W₂C above 500 °C during HVOF, reducing the wear resistance of such coatings and limiting their application (Ref 17–19). Meanwhile, Cr₃C₂-NiCr ceramic-metallic coatings show better thermal stability and oxidation resistance due to formation of dense Cr₂O₃ film on the surface (Ref 20). Yang et al. (Ref. 21) claimed that Cr₃C₂-NiCr ceramic-metallic coatings showed less hardness decrease at temperature above 600 °C and retained good erosion resistance up to 800 °C in working conditions. Therefore, Cr₃C₂-NiCr ceramic-metallic coatings are commonly used for workpieces for operation under harsh wear conditions, especially at medium or high temperature (Ref 22, 23).

In the present work, to obtain HVOF coatings with high adhesion strength on Cu matrix, three types of bond layers

between the HVOF cermet layer and Cu matrix were designed and produced, i.e., electroplated Ni, HVOF-sprayed NiCr, and double-decker Ni-NiCr. In addition, annealing was performed to further enhance the adhesion strength. The microstructure of the deposited coatings was systematically investigated by x-ray diffraction analysis and scanning electron microscopy. Their mechanical properties were also measured.

Experimental Procedures

Coating Design and Deposition

Three different types of GC with different metallic bond layers were designed (Fig. 1). The metallic bond layers of the three GCs were HVOF-sprayed NiCr on electroplated Ni, electroplated Ni, and HVOF-sprayed NiCr. Then, a NiCr-30 wt.%Cr₃C₂ cermet layer was sprayed on each metallic bond layer by HVOF. The spraying parameters for the NiCr metallic bond layer and top cermet layer are specified in Table 1. A WOKA-Star 600 HVOF spraying system (Sulzer Metco Inc., Westbury, NY, USA) was used. The spraying powders were commercial NiCr alloy (Sulzer Metco, Westbury, NY, USA) and NiCr-30 wt.%Cr₃C₂ supplied by mixing NiCr-75Cr₃C₂ sinter fines (Sulzer Metco, Westbury, NY, USA) and NiCr alloy. The morphology of the different powders is shown in Fig. 2. The spheroidal NiCr and NiCr-75Cr₃C₂ powder exhibited

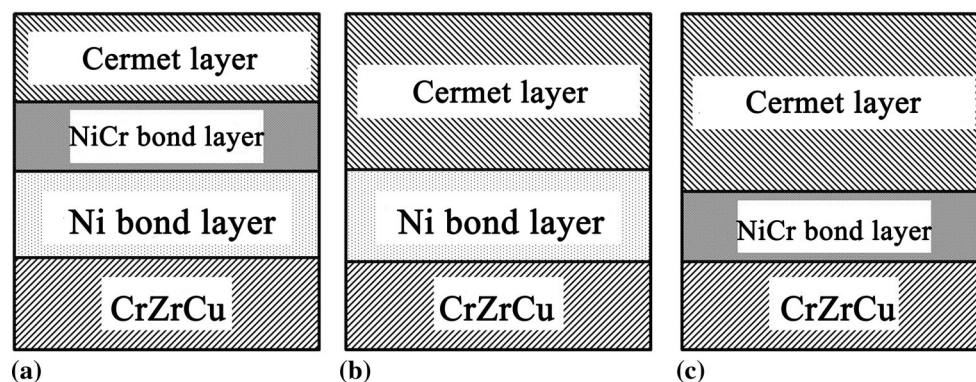


Fig. 1 Schematic diagram of NiCr-30 wt.%Cr₃C₂ cermet layer sprayed on three types of metallic bond layers: (a) GC-Ni-NiCr, (b) GC-Ni, and (c) GC-NiCr, where “GC” indicates gradient coating

Table 1 HVOF spraying parameters for NiCr metallic and NiCr-30 wt.%Cr₃C₂ cermet layers

Parameter	Oxygen (NLPM)	Fuel, L/h	Combustion Pressure, bar	Powder Feed Rate, g/min	Spray Distance, mm
NiCr-30 wt.%Cr ₃ C ₂	876	23.1	10.1	29 × 2	340
NiCr	876	23.1	10.1	29 × 2	340

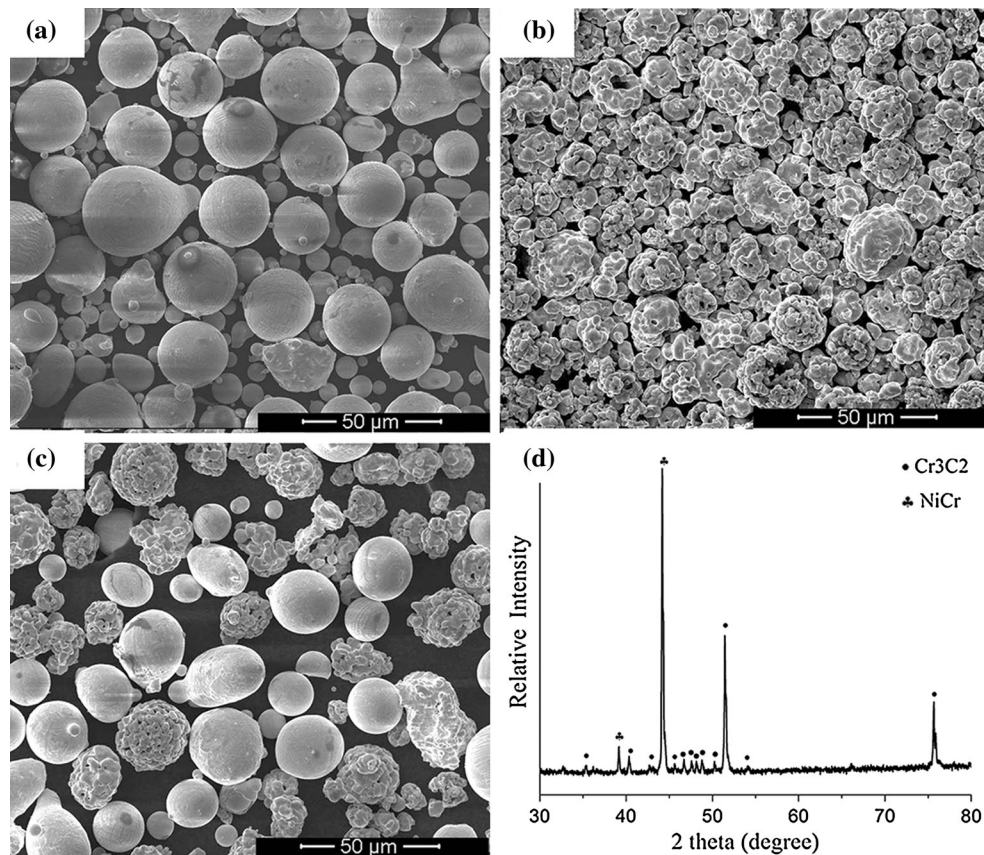


Fig. 2 Morphology of powders: (a) NiCr alloy, (b) NiCr-Cr₃C₂ sinter fines, and (c) NiCr-30 wt.%Cr₃C₂ spraying powder. (d) XRD pattern of NiCr-30 wt.%Cr₃C₂ spraying powder

particle size range of $45 \pm 15 \mu\text{m}$ in diameter and the NiCr-30 wt.%Cr₃C₂ powder was mixed uniformly, as seen in Fig. 2(c). Figure 2(d) shows that the main phases of the spraying powder were NiCr and Cr₃C₂.

The GCs were deposited onto 100 mm × 20 mm × 5 mm CrZrCu alloy for microstructure characterization and wear testing, and then onto Ø25 mm CrZrCu cylinders for adhesion testing. Before spraying the GCs, the substrate or electroplated Ni metallic bond layer was degreased with acetone and grit-blasted with white corundum at 5.6 bar, 90° blasting incidence angle, and blasting distance of about 250 mm. The grit-blasted substrate or electroplated Ni metallic bond layer had mean roughness (R_a) of 3.2 μm .

For convenience, the gradient coatings (GCs) on double-decker Ni-NiCr, Ni, and NiCr metallic bond layers are denoted as GC-Ni-NiCr, GC-Ni, and GC-NiCr, respectively.

It is noteworthy that, to avoid electroplating, which is harmful to the environment, the GC-NiCr coating was designed without an electroplated Ni bond layer. Meanwhile, the GC-NiCr coating was annealed at 800, 850, or 900 °C for 2 h in nitrogen atmosphere to enhance the adhesion strength and wear resistance.

Microstructure Characterization

X-ray diffraction (XRD) analysis (Bruker D8 Advance) was employed to analyze the phase composition of the different coatings. The Bruker D8 diffractometer was operated at 40 kV and 40 mA using Cu K α radiation. The scan speed was 2°/min in the 2 θ range from 30° to 80°. The cross-sectional morphology of the coatings was studied by scanning electron microscopy (SEM, JSM-6490LV) equipped with energy-dispersive x-ray (EDX) microanalysis.

Adhesion Testing

The adhesion of the coating systems was measured according to ASTM adhesion test standard (Ref 24). The adhesive used in the adhesion test was HTK Ultrabond 100 (HTK Hamburg, Hamburg-Sasel, Germany), whose highest strength is about 70 MPa, cured at 180 °C and 20 N pressure for 1 h. The adhesion strength was calculated using the equation $R_h = F_m/S$, where R_h is the adhesion strength, F_m is the maximum load, and S is the fracture cross-sectional area. The bond strength type was determined according to the failure location.

Microhardness Measurements

The microhardness of the coatings including the cermet layer, metallic bond layer, and substrate was determined at load of 500 g using a Matsuzawa MTX- α microhardness tester. The values quoted are averages of ten measurements on each coating in different areas.

Wear Testing

Wear tests were carried out on polished GCs using a ball-on-disk (BOD) device (HT3001) using the test parameters listed in Table 2. The wear counterpart was 40Cr, whose hardness is about HRC 45, with diameter of 6 mm. The three dimensions (3D) topography of the wear scars was measured using a KLA-Tencor P7 step profiler, and the worn morphology was obtained by SEM. The wear rate was calculated using the formula

$$k = \frac{W_v}{L \times s d},$$

where L is the load (N), W_v is the wear volume (m^{-3}), s is the distance per circle, and d is the number of circles.

Results and Discussion

Phase and Microstructure of Coatings

Figure 3 shows the XRD patterns of the GCs with different types of bond layer and the annealed GC-NiCr coating. As

shown in Fig. 3(a), the XRD patterns of the as-sprayed coatings revealed that they were mainly composed of NiCr and Cr_3C_2 . However, the Cr_7C_3 peak intensity was slightly greater in comparison with the XRD pattern of the spraying powder (Fig. 3a, magnified part), implying that little phase transformation of Cr_3C_2 to Cr_7C_3 occurred during the spraying process (Ref 25), perhaps due to the high velocity of the particle spraying process. The peak at around 35° in Fig. 3(a) indicates that little Cr was oxidized to Cr_2O_3 in the HVOF spraying process. As shown in Fig. 3(b), the main phases of the coatings were NiCr, Cr_3C_2 , and Cr_7C_3 , while the Cr_7C_3 peak intensity increased with increasing annealing temperature, indicating phase transformation from Cr_3C_2 to Cr_7C_3 during the annealing treatment (Ref 26). Compared with the as-sprayed GC-NiCr coating, a peak appears at around 57° after annealing in Fig. 3(b), indicating that Cr_2O_3 formed during annealing treatment.

The cross-sectional morphology of all the coatings was analyzed by SEM using backscattered electron (BSE) imaging. Figure 4 shows the cross-sectional morphology of the three types of GC, while the GC-NiCr coating before and after annealing is shown in Fig. 5. The microstructure of the HVOF-sprayed coatings, including the NiCr bond layer and the NiCr-30 wt.% Cr_3C_2 cermet coating, revealed classic plate-type structure as shown in Fig. 4 and 5. The phase of the cermet coating was NiCr with inserted Cr-based carbide. The reason is that the spraying powder for the cermet coating was formed of NiCr- Cr_3C_2 sinter fines mixed among NiCr alloy powder and the fusion point of Cr_3C_2 is higher than that of NiCr. Figure 4(b) shows

Table 2 Parameters for ball-on-disk wear tests

Load, N	Diameter, mm	Time, s	Temperature, $^\circ\text{C}$	Relative humidity (RH)	Wear speed, r/min
20	6	3600	20	50 ± 5	200

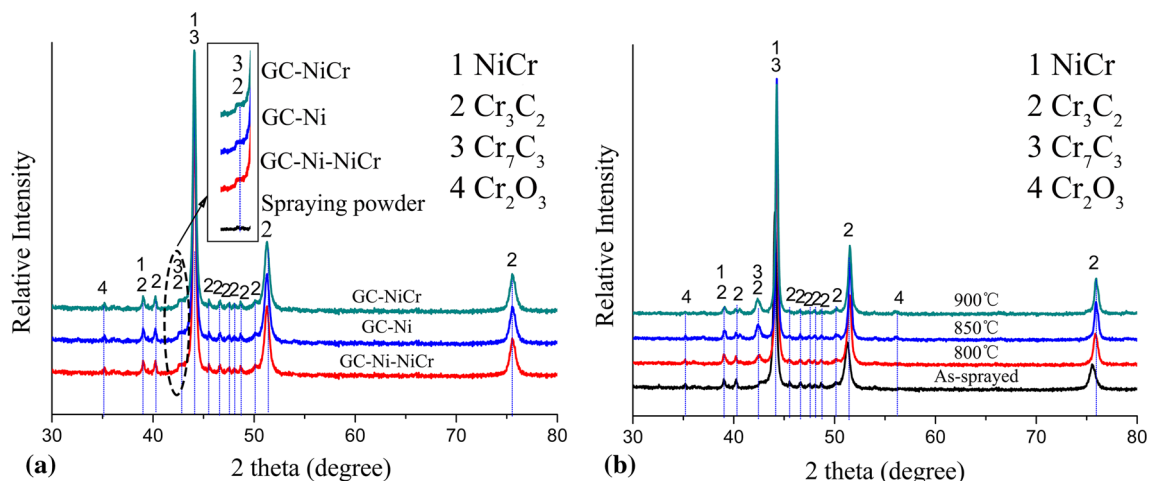


Fig. 3 XRD patterns of (a) coatings with different metallic bond layers, and (b) GC-NiCr coating before and after annealing treatment

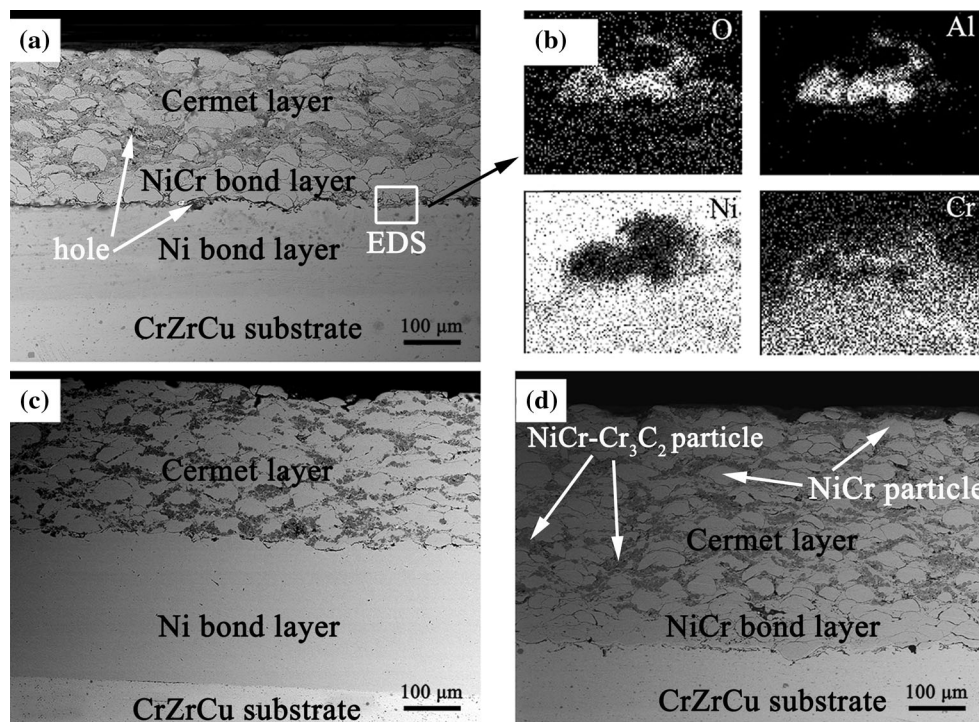


Fig. 4 Cross-sectional morphology of coatings with different metallic bond layers: (a) GC-Ni-NiCr coating with (b) element mapping of marked area, (c) GC-Ni coating, and (d) GC-NiCr coating

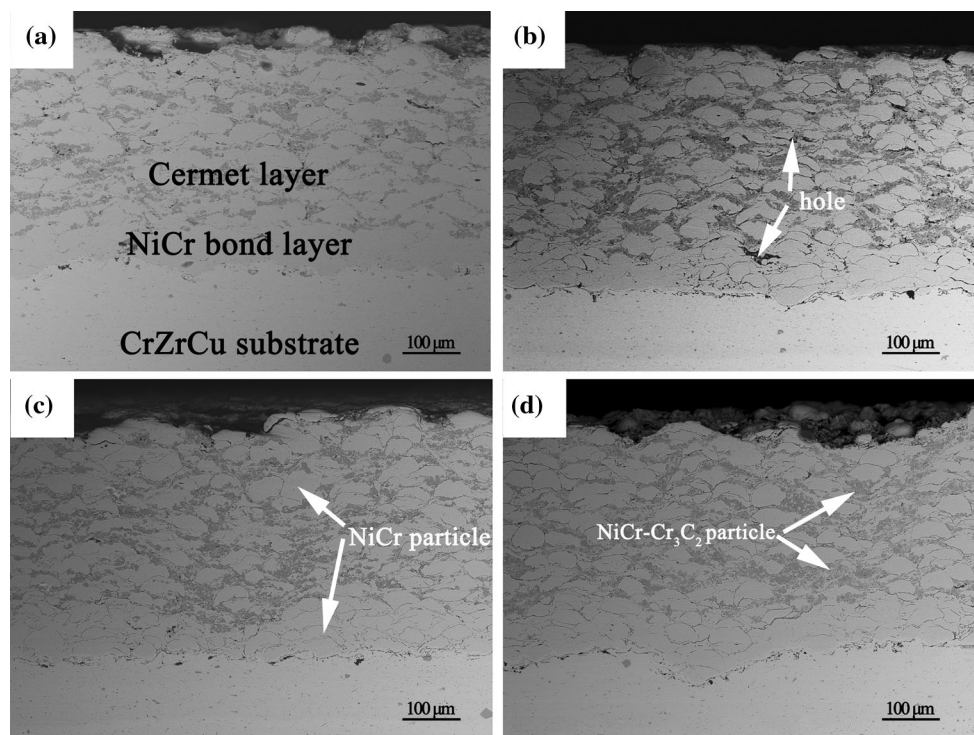


Fig. 5 Cross-sectional morphology of GC-NiCr coating (a) as-sprayed, and annealed at (b) 800 °C, (c) 850 °C, and (d) 900 °C

elemental mapping of the area marked in Fig. 4(a), revealing a “rat”-like shape in the Al and O maps. This indicates that a small amount of Al oxides occurred at the

interface of the NiCr and electroplated Ni, probably due to contamination by corundum before HVOF spraying of the NiCr metallic bond layer.

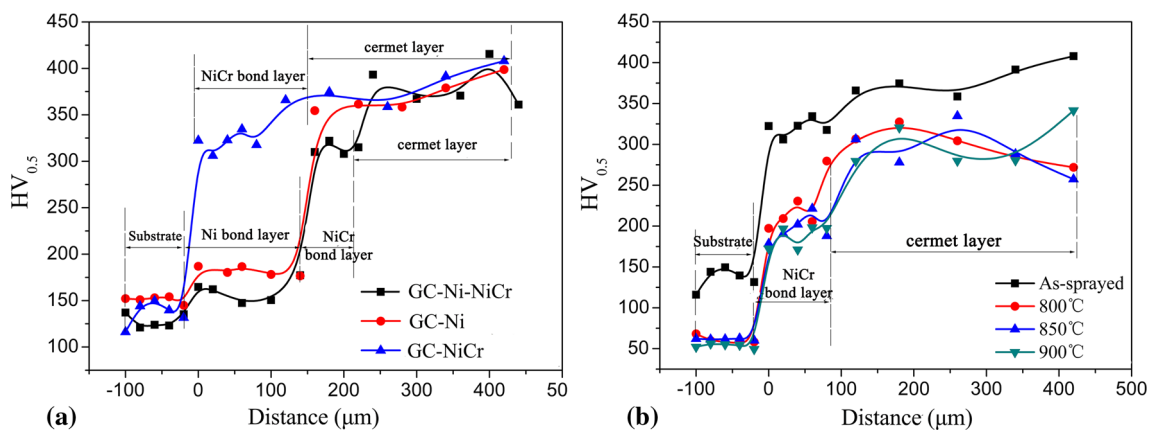


Fig. 6 Microhardness variation from inner substrate to exterior cermet layer for (a) coatings with three types of metallic bond layer, and (b) GC-NiCr coating before and after annealing treatment

Microhardness

The cross-section microhardness of the as-sprayed GCs is shown in Fig. 6(a). For the GC-Ni-NiCr coating, the microhardness transition from the substrate to cermet layer was gradual. In contrast, the microhardness differences were relatively large from both the substrate to the NiCr metallic bond layer and from the Ni metallic bond layer to the cermet layer. The microhardness variation from the inner substrate to the exterior cermet layer before and after annealing is shown in Fig. 6(b), from which it can be concluded that the microhardness of the cermet layer was almost 420 HV, decreasing to 350 HV after annealing. The variation of the measured values was large because of the low content and the distribution of Cr_3C_2 particles inserted in the NiCr matrix. The decrease in the microhardness can be attributed to the distribution of Cr_3C_2 , grain coarsening of the NiCr metallic bond layer, and the CrZrCu substrate.

Adhesion Strength

One of the most important factors in thermal spray coating is adhesion strength, being directly related to the coating durability (Ref 27). It has been confirmed that the main adhesion mechanism of HVOF-sprayed coatings is mechanical interlocking, which is affected by roughness, spraying distance, oxygen flow, etc. (Ref 28). The adhesion strength and failure location of the coatings with different metallic bond layers according to the adhesion test results are presented in Table 3, from which it can be seen that the adhesion strength of the GC-Ni-NiCr, GC-Ni, and GC-NiCr coatings was 24, 69, and 15 MPa, with failure location at the T/E, W/E, and T/S interface, respectively (where “T” indicates the NiCr bond layer, “W” the cermet layer, “E” the Ni bond layer, and “S” the substrate). Based on the adhesion strength and failure location for the different coatings in Table 3, the adhesion strength of T/S (15 MPa)

Table 3 Adhesion strength and failure location of coatings with different metallic bond layers

Gradient coating	GC-Ni-NiCr	GC-Ni	GC-NiCr
Adhesion strength, MPa	24	69	15
Failure location	T/E	W/E	T/S

T NiCr bond layer, W cermet layer, E Ni bond layer, S substrate

was weaker than that at T/E (24 MPa) and W/E (69 MPa). From the failure location of the GC-Ni coating, it can be concluded that the adhesion strength of E/S was better than W/E, and a similar conclusion can be reached for higher adhesion strength of W/E than T/E by comparing the failure of the GC-Ni-NiCr coating. In summary, the strength between the layers of the coatings decreased in the order E/S, W/E, T/E, T/S in the as-sprayed condition. Figure 7 shows the microstructure of various interfaces. As shown in Fig. 7(a), the T/E and T/S interfaces contained more defects, implying poor adhesion. Meanwhile, Fig. 7(b) and (c) reveals that there were fewer defects at the W/E and W/T interfaces, while Cr_3C_2 particles played a pinning role, resulting in better adhesion. In addition, research has shown that the size of the spraying powder has a great effect on the melted fraction (Ref 34). In the present NiCr bond layer spraying process, different melting fraction of NiCr particles would result in more defects (holes marked in Fig. 7) at the T/E and T/S interfaces, where failure took place easily.

The adhesion strength and failure location for the GC-NiCr coating with annealing treatment are presented in Table 4. Obviously, the adhesion strength increased significantly while the failure location was at the glue after annealing, indicating that annealing improved the adhesion of the T/S interface and the actual adhesion was even higher than the test result. As shown in Fig. 8, it can be

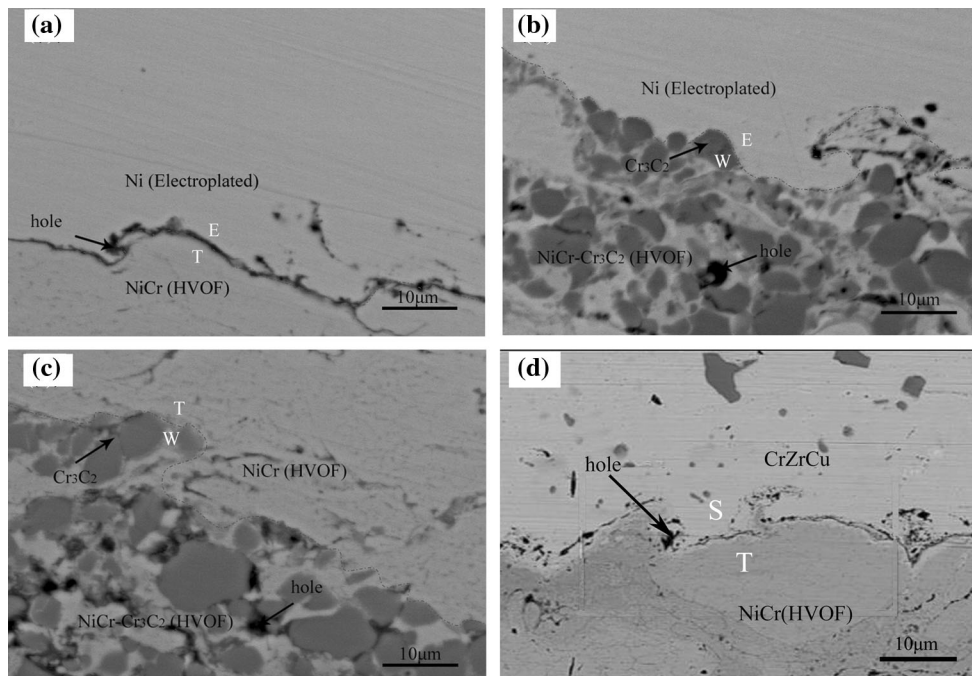


Fig. 7 Morphology of various interfaces: (a) Ni and NiCr bond layers, (b) Ni bond layer and cermet layer, (c) NiCr bond layer and cermet layer, and (d) CrZrCu substrate and NiCr bond layer

Table 4 Adhesion strength and failure location of GC-NiCr coatings before and after annealing

Annealing temperature, °C	As-sprayed	800	850	900
Adhesion strength, MPa	15	73	71	74
Failure location	T/S	G	G	G

T NiCr bond layer, S substrate, G glue

hypothesized that high-temperature annealing promoted elemental diffusion, thereby enhancing the adhesion at the NiCr and CrZrCu substrate interface. In addition, relief or conversion of residual stress due to nonequilibrium crystallization and structure could be an important effect improving the adhesion strength (Ref 29, 30).

Wear Resistance

The wear resistance of a thermally sprayed coating is a comprehensive performance measure that depends on several factors including microstructure, hardness, toughness, etc. (Ref 31). The 3D topography of the GCs with different metallic bond layers is shown in Fig. 9. The maximum wear scar depth of about 70 µm was found for the GC-Ni-NiCr coating, as shown in Fig. 9(a). The thickness of the cermet layer was almost 200-330 µm (Fig. 4 and 5), indicating that the cermet layer was not worn away. As shown in Fig. 9, the bottom of all the wear

scars was rugged, indicating that the high-hardness Cr₃C₂ distributed in a dispersed fashion in the NiCr matrix increased the loading capacity of the coating. The wear morphology of all the GCs is shown in Fig. 10(a)-(f), all being nearly the same, covered with wear debris. Figure 11 shows the wear morphology of the cermet layer and wear counterpart, while Table 5 presents the element micro-analysis results for the areas marked in Fig. 11. The results in Table 5 show that area A contained large amounts of Fe and O, while area B contained more Ni and Cr, with much C and O elements in area C. During the wear process, plastic deformation of the softer NiCr phase in the cermet layer occurred under the loading force, followed by flattening or tearing under the action of tangential stress (crack shown in Fig. 11a). At the same time, Cr₃C₂ particles were exposed and stripped out, being retained in the wear counterpart. With the ongoing wear process, Cr and Fe elements were oxidized at the high temperature caused by the high wear speed. Therefore, the main wear mechanism was adhesive wear as well as oxidation wear.

As mentioned above, comparing the microhardness (Fig. 6) with the wear rate (Fig. 12) results reveals that the microhardness values of all the obtained cermet layers were at a similar level, while the wear rate in the as-sprayed condition was very different, with the GC-NiCr coating exhibiting the best wear resistance and the GC-Ni-NiCr coating the worst. Meanwhile, for the GC-NiCr coating, although the microhardness of the cermet layer, metallic bond layer, and substrate all decreased after

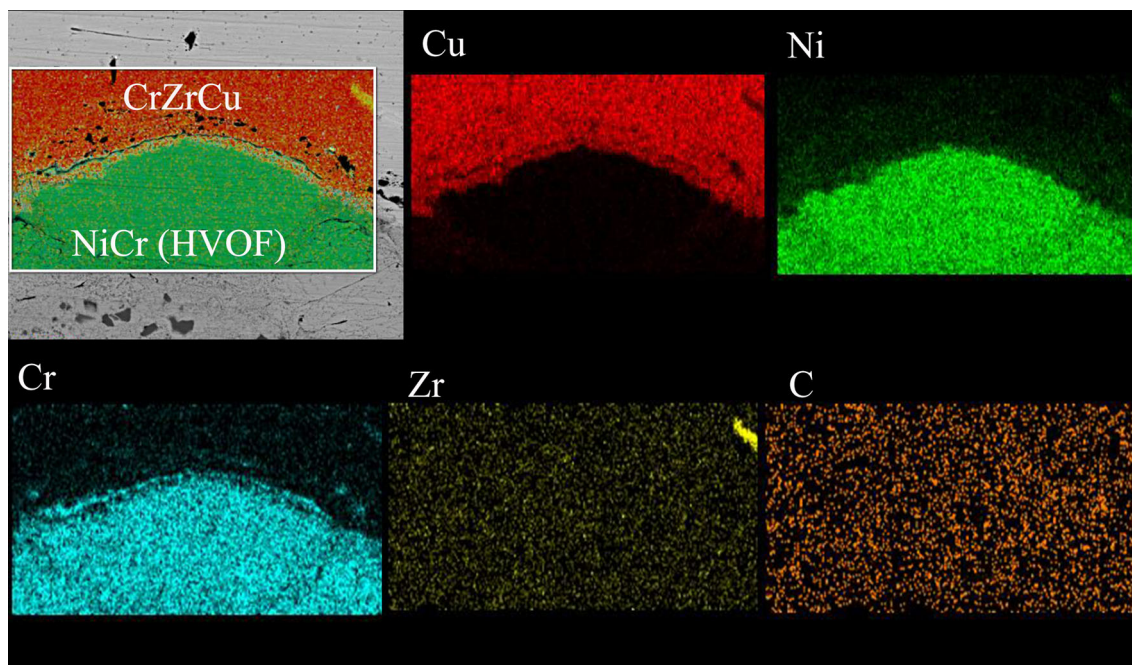


Fig. 8 EPMA maps of CrZrCu substrate and NiCr bond layer

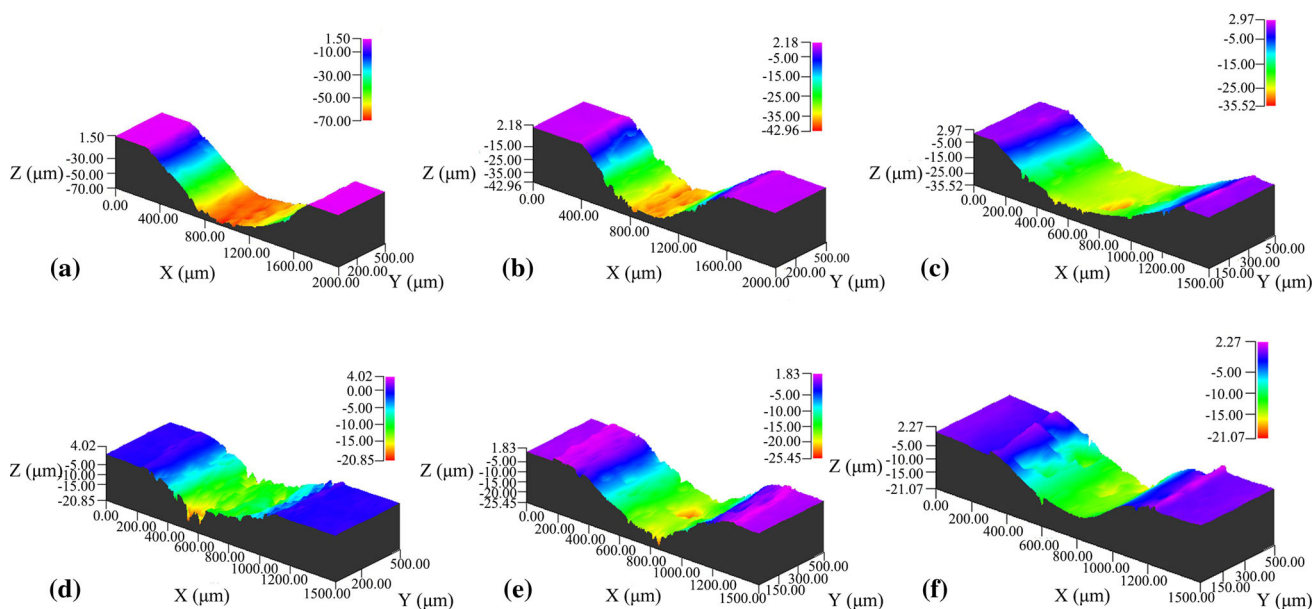


Fig. 9 Three dimensions topography of GCs with different metallic bond layers: (a) GC-Ni-NiCr coating, (b) GC-Ni coating, (c) GC-NiCr coating, and GC-NiCr coatings annealed at (d) 800 °C, (e) 850 °C, and (f) 900 °C

annealing, the wear resistance improved. Therefore, the wear resistance of the designed GCs showed no correlation with the microhardness of the top cermet layer but rather with the type of metallic bond layer and annealing treatment applied. The residual stress in HVOF coatings is tensile due to the mismatch between the coating and substrate (Ref 32), being detrimental to the wear resistance of the coating. However, after annealing treatment, the

residual stress was relieved or even converted to compressive due to the high-temperature heat treatment; compressive stress is beneficial for the wear resistance of HVOF coatings (Ref 33). Thus, such relief or conversion of the tensile stress of the HVOF coating is the main reason for the wear rate decrease after annealing treatment. On the other hand, plastic deformation of the NiCr phase becomes easier and the NiCr metallic bond layer could be more

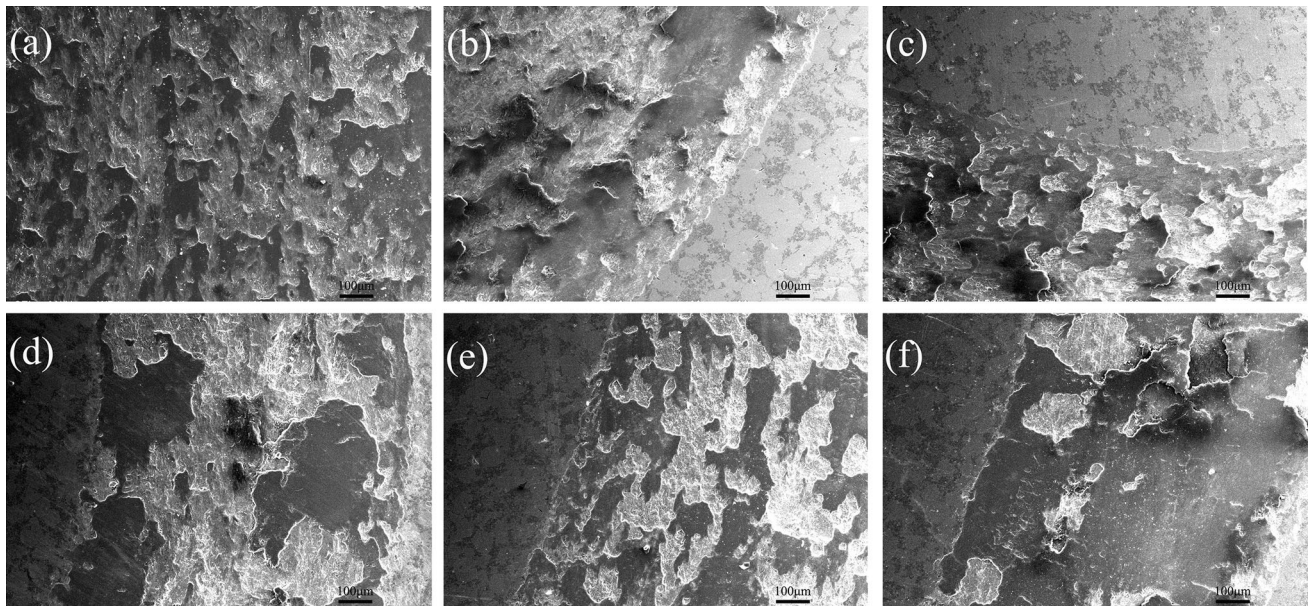


Fig. 10 Wear morphology of coatings with different metallic bond layers: (a) GC-Ni-NiCr coating, (b) GC-Ni coating, (c) GC-NiCr coating, and GC-NiCr coatings annealed at (d) 800 °C, (e) 850 °C, and (f) 900 °C

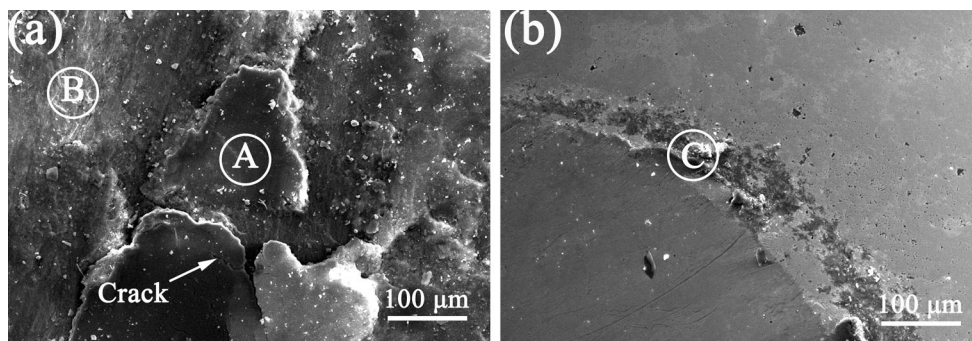


Fig. 11 Wear morphology of (a) cermet layer and (b) wear counterpart

Table 5 Elemental microanalysis results for marked areas in wear scar and counterpart

Element	C	O	Cr	Fe	Ni
Point A, wt.%	13.79	30.03	4.33	46.12	5.72
Point B, wt.%	2.32	12.71	20.46	2.73	60.77
Point C, wt.%	31.63	32.73	12.88	10.96	11.79

compact, while the structure could become denser at the same time, as could be observed from the lower depth of the wear scar after annealing treatment (as shown in Fig. 9c-f). During the wear test, more area of the NiCr matrix was flattened (as shown in Fig. 10c-f), resulting in more hard Cr₃C₂ particles inserted more tightly in the NiCr matrix. Consequently, the supporting Cr₃C₂ particles inserted into the NiCr matrix improved the wear resistance of the GC-NiCr coating. The exact relationship between the

wear resistance and the type of metallic bond layer is under further study.

Conclusions

NiCr-30 wt.%Cr₃C₂ cermet coatings were sprayed by HVOF on copper alloy substrate using various bond layers. The microstructure and properties of the different coatings were investigated systematically. The main results can be summarized as follows:

1. The microhardness of the GC showed a decreasing trend from the top ceramic coating (about HV 420) to the substrate, and a few Cr₃C₂ particles decomposed to Cr₇C₃ during the spraying process.
2. The adhesion of the GC to the Ni bond layer was highest (about 70 MPa) due to better mechanical interlocking and fewer defects. The adhesion strength

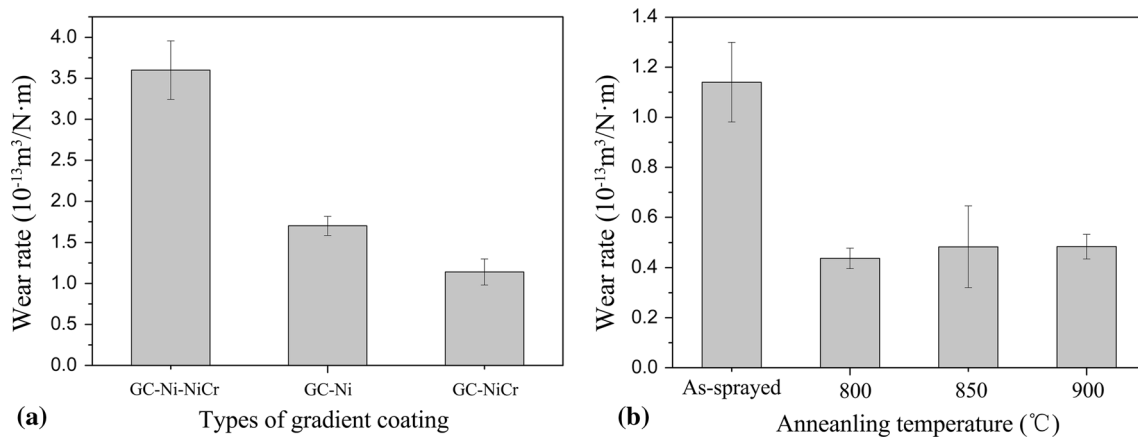


Fig. 12 Wear rates of (a) GCs with three types of metallic bond layer and (b) GC-NiCr coating before and after annealing treatment

of the coating with the NiCr metallic bond layer exhibited an obvious increase after annealing.

- The GC on the NiCr metallic bond layer exhibited the best wear resistance in as-sprayed condition. Moreover, its wear resistance was significantly improved by annealing due to relief or conversion of the internal stress in the coating, plastic deformation of the NiCr phase, denser structure, and high loading capacity of the NiCr-30 wt.%Cr₃C₂ cermet layer.

Acknowledgments This work was supported by the National Science Foundation of China (Grant No. 51671002) and the Key Technology Program of Anhui Province (Grant No. 1501021065).

Reference

- Y.M. Won, T.J. Yeo, K.H. Oh, J.K. Park, J. Choi, and C.H. Yim, Analysis of Mold Wear During Continuous Casting of Slab, *ISIJ Int*, 1998, **38**(1), p 53-62
- A. Sanz, Tribological Behavior of Coatings for Continuous Casting of Steel, *Surf Coat Technol*, 2001, **146**, p 55-64
- N.E. Fenineche, R. Hamzaoui, and O. El Kedim, Structure and Magnetic Properties of Nanocrystalline Co-Ni and Co-Fe Mechanically Alloyed, *Mater Lett*, 2003, **57**(26), p 4165-4416
- H.J.C. Voorwald, R. Padilha, M.Y.P. Costa, W.L. Pigatin, and M.O.H. Cioffi, Effect of Electroless Nickel Interlayer on the Fatigue Strength of Chromium Electroplated AISI, 4340 Steel, *Int J Fatigue*, 2007, **29**(4), p 695-704
- G.C. Ji, C.J. Li, Y.Y. Wang, and W.Y. Li, Erosion Performance of HVOF Sprayed Cr₃C₂-NiCr Coatings, *J Therm Spray Technol*, 2007, **16**(4), p 557-565
- W. Fang, T.Y. Cho, J.H. Yoon, K.O. Song, S.K. Hur, S.J. Youn, and H.G. Chun, Processing Optimization, Surface Properties and Wear Behavior of HVOF Spraying WC-CrC-Ni Coating, *J Therm Spray Technol*, 2009, **209**(7), p 3561-3567
- Q. Wang, Z.H. Chen, and Z.X. Ding, Performance of Abrasive Wear of WC-12Co Coatings Sprayed by HVOF, *Tribol Int*, 2009, **42**(7), p 1046-1051
- C.B. Huang, L.Z. Du, and W.G. Zhang, Microstructure, Mechanical and Tribological Characteristics of Plasma, Detonation Gun and HVOF Sprayed NiCr/Cr₃C₂-BaF₂Ca-F2 Coatings, *Surf Eng*, 2011, **27**(10), p 762-769
- M.X. Xie, S.H. Zhang, and M.X. Li, Comparative Investigation on HVOF Sprayed Carbide-Based Coatings, *Appl Surf Sci*, 2013, **273**, p 799-805
- H. Mizuno and J. Kitamura, MoB/CoCr Cermet Coatings by HVOF Spraying Against Erosion by Molten Al-Zn Alloy, *J Therm Spray Technol*, 2007, **16**(3), p 404-413
- E. Celik, O. Culha, B. Uyulgan, N.F. AkAzem, I. Ozdemir, and A. Turk, Assessment of Microstructural and Mechanical Properties of HVOF Sprayed WC-Based Cermet Coatings for a Roller Cylinder, *Surf Coat Technol*, 2006, **200**(14), p 4320-4328
- A. Sanz, New Coatings for Continuous Casting Rolls, *Surf Coat Technol*, 2004, **177**, p 1-11
- L. Zhu, L. Zhang, S. Zhao, and J. Wang, Analysis of Microstructure and Properties of WC-12Co Coating Sprayed by High Velocity Oxygen Fuel on the Surface of Continuous Casting Mold, *Foundry Technol.*, 2011, **2**(32), p 242-247
- G. Barbezat, J.R. Moens, and A.R. Nicoll, Properties and Applications of CDS Coatings, *Mater Des*, 1992, **13**(3), p 145-148
- T. Sahraoui, N.E. Fenineche, G. Montavon, and C. Goddet, Structure and Wear Behaviour of HVOF Sprayed Cr₃C₂-NiCr and WC-Co Coatings, *Mater Des*, 2003, **24**(5), p 309-313
- D. Toma, W. Brandl, and G. Marginean, Wear and Corrosion Behavior of Thermally Sprayed Cermet Coatings, *Surf Coat Technol*, 2001, **138**(2), p 149-158
- E. Zdravecka, J. Suchanek, J. Tacova, J. Trpcevska, and K. Brinkienė, Investigation of Wear Resistance of High Velocity Oxy-Fuel Sprayed WC-Co and Cr₃C₂-NiCr Coatings, *Mechanika*, 2010, **4**(84), p 75-79
- M. Kaur, H. Singh, and S. Prakash, High-Temperature Corrosion Studies of HVOF-Sprayed Cr₃C₂-NiCr Coating on SAE-347H Boiler Steel, *J Therm Spray Technol*, 2009, **18**(4), p 619-632
- Š. Houdková, F. Zahálka, M. Kašparová, and L.M. Berger, Comparative Study of Thermally Sprayed Coatings Under Different Types of Wear Conditions for Hard Chromium Replacement, *Tribol Lett*, 2011, **43**(2), p 139-154
- H.S. Sidhu, B.S. Sidhu, and S. Prakash, Hot Corrosion Behavior of HVOF Sprayed Coatings on ASTM SA213-T11 Steel, *J Therm Spray Technol*, 2007, **16**(3), p 349-354
- G.J. Yang, C.J. Li, S.J. Zhang, and C.X. Li, High-Temperature Erosion of HVOF Sprayed Cr₃C₂-NiCr Coating and Mild Steel for Boiler Tubes, *J Therm Spray Technol*, 2008, **17**(5-6), p 782-787
- G. Sun, Y. Zhang, C. Liu, X. Tao, and P. Li, Microstructure and Wear Resistance Enhancement of Cast Steel Rolls by Laser

- Surface Alloying NiCr-Cr₃C₂, *Mater Des*, 2010, **31**(6), p 2737-2744
23. C.B. Huang, L.Z. Du, and W.G. Zhang, Preparation and Characterization of Atmospheric Plasma Sprayed NiCr/Cr₃C₂-BaF₂-CaF₂ Composite Coating, *Surf Coat Technol*, 2009, **203**(20-21), p 3058-3065
 24. Standard test method for adhesion or cohesion strength of thermal spray coatings C 633-79, *Annual Book of ASTM Standards*, Part 17 (ASTM, 1982), pp. 636-642
 25. S. Hong, Y. Wu, and Q. Wang, Microstructure and Cavitation–Silt Erosion Behavior of High-Velocity Oxygen–Fuel (HVOF) Sprayed Cr₃C₂-NiCr Coating, *Surf Coat Technol*, 2013, **225**, p 85-91
 26. J.K.N. Murthy, K.S. Prasad, and K. Gopinath, Characterization of HVOF Sprayed Cr₃C₂-50(Ni20Cr) Coating and the Influence of Binder Properties on Solid Particle Erosion Behavior, *Surf Coat Technol*, 2010, **204**(24), p 3975-3985
 27. Y.Y. Wang, C.J. Li, and A. Ohmori, Examination of Factors Influencing the Bond Strength of High Velocity Oxy-Fuel Sprayed Coatings, *Surf Coat Technol*, 2006, **200**(9), p 2923-2928
 28. M. Watanabe, A. Owada, S. Kuroda, and Y. Gotoh, Effect of WC Size on Interface Fracture Toughness of WC-Co HVOF Sprayed Coatings, *Surf Coat Technol*, 2006, **201**(3), p 619-627
 29. M.H. Staia, E. Ramos, and A. Carrasquero, Effect of Substrate Roughness Induced by Grit Blasting Upon Adhesion of WC-17% Co Thermal Sprayed Coatings, *Thin Solid Films*, 2000, **377**, p 657-664
 30. C.S. Richard, G. Beranger, and J. Lu, The Influences of Heat Treatments and Inter Diffusion on the Adhesion of Plasma Sprayed NiCrAlY Coatings, *Surf Coat Technol*, 1996, **82**(1-2), p 99-109
 31. A. Mateen, G.C. Saha, T.I. Khan, and F.A. Khalid, Tribological Behavior of HVOF Sprayed Near-Nanostructured and Microstructure WC-wt.17%Co Coatings, *Surf Coat Technol*, 2011, **206**(6), p 1077-1084
 32. J. Stokes and L. Looney, Residual Stress in HVOF Thermally Sprayed Thick Deposits, *Surf Coat Technol*, 2004, **177**, p 18-23
 33. D.A. Stewart, P.H. Shipway, and D.G. McCartney, Influence of Heat Treatment on the Abrasive Wear Behaviour of HVOF Sprayed WC-Co Coatings, *Surf Coat Technol*, 1998, **105**(1), p 13-24
 34. H. Li, K.A. Khor, and P. Cheang, Adhesive and Bending Failure of Thermal Sprayed Hydroxyapatite Coatings: Effect of Nanostructures at Interface and Crack Propagation Phenomenon During Bending, *Eng Fract Mech*, 2007, **74**(12), p 1894-1903